Generation of Femtosecond Optical Vortex Beams in All-Fiber Mode-Locked Fiber Laser Using Mode Selective Coupler

Teng Wang, Feng Wang, Fan Shi, Fufei Pang, Sujuan Huang, Tingyun Wang, and Xianglong Zeng

***Abstract*—We experimentally demonstrated a high-order optical vortex pulsed laser based on a mode selective all-fiber fused coupler composed of a single-mode fiber (SMF) and a few-mode fiber (FMF). The fused SMF-FMF coupler inserted in the cavity acts as a mode converter from LP_{01} mode to LP_{11} (LP_{21}) mode with a broadband width. Linearly polarized OAM modes can be obtained by combining different vector modes $HE_{2,m}^{even}$ ($HE_{2,m}^{odd}$) and $TE_{0,m}$ ($TM_{0,m}$) when $l = 1$ or combining $HE_{l+1,m}^{even}$ ($HE_{l+1,m}^{odd}$) and $EH_{l-1,m}^{odd}$ ($EH_{l-1,m}^{even}$) when $l > 1$ with a $\pi/2$ phase shift. To the best of our knowledge, this is the first report on the generation of high-order pulse vortex beams in a mode-locked fiber laser. The measured time duration of OVB pulses is 273 fs, 140 fs of $OAM_{\pm 1}$ and $OAM_{\pm 2}$.**

***Index Terms*—Fiber lasers, mode selective coupler, optical vortices, orbital angular momentum, ultrafast optics.**

I. Introduction

OPTICAL vortex beams (OVBs), also called orbital angular momentum (OAM) beams, are spatially structured beams with helical phase front. Such beams are characterized by a topological charge (order), and are found to carry an OAM of *lh* per photon, where *l* is referred as the topological charge and can take any integer value, *h* is the reduced Planck constant [1]. In the analytic expression, this helical phase front is usually related to a phase term of $\exp(il\theta)$ in the transverse plane, where θ refers to the azimuthal coordinate and l is an integer counting the number of intertwined helices. Therefore l can be assumed as a positive, negative or zero value, corresponding to clockwise or counterclockwise phase helices or a Gaussian beam, respectively [2]. As vortex beams have a phase singularity, they have a doughnut-shaped spatial profile with zero intensity at the center. Due to the doughnut spatial structure and OAM properties, optical vortex beams attract a lot of attention in view of their applications, including optical tweezers [3], particle trapping [4], quantum computation [5], data transmission [6], optical communications [7], [8] and material processing [9]–[13].

Driven by the distinctive properties and miscellaneous applications, there have been many attempts to generate optical vortex beams. Different methods to generate optical vortices both in free space and optical fibers have been proposed: spiral phase plates [14], spatial light modulator (SLM) [15], computer-generated holograms [16], cylindrical lens pairs [17], Q-plates [18], gratings technique [19]–[22], couplers [23], [24] and so on. All of these methods to generate optical vortices are investigated by using a continuous wave (CW), but many applications require OVBs with an ultrahigh peak power and narrow temporal pulse duration, such as in the field of material processing [11]. Several attempts to generate pulsed OVBs have been reported. Recent years, Jianlang Li *et al.* reported a radially polarized and passively Q-switched Yb-doped fiber laser. By using a Cr^{4+}:YAG crystal as a saturable absorber and a photonic crystal grating as a polarization mirror, a radially polarized pulse is produced [25]–[27]. But the scheme is not an all-fiber system which is not conducive to the integration of fiber system. Jiangli Dong *et al.* demonstrated a passively mode-locked fiber laser that incorporates a two-mode fiber Bragg grating (FBG) for transverse-mode selection. When the laser is mode-locked, it generates picosecond pulses at a fundamental repetition rate of 6.58 MHz for both the LP_{01} and LP_{11} modes [28]. However, it is known that the fiber grating only possesses narrow reflection bandwidth, which limits available spectrum of OVBs pulses. Thus using the fiber grating is difficult for achieving femtosecond pulse duration. In order to generate a laser pulse within femtosecond time domain, it needs using a broad spectral bandwidth of mode conversion. Mode selective coupler (MSC) can work well at a broadband width. Therefore generating femtosecond vortex pulse is preferred based on fiber laser by using a mode selective coupler.

In this paper, we present an all-fiber mode-locked fiber laser (MLFL) with femtosecond OVB pulse based on nonlinear polarization rotation (NPR) [29]. A fused SMF-FMF coupler is tactfully exploited to deliver pulse energy out of the fiber cavity, at the same time to achieve the mode conversion from LP_{01}

Manuscript received September 19, 2016; revised January 18, 2017 and February 20, 2017; accepted February 24, 2017. Date of publication February 28, 2017; date of current version April 20, 2017. This work was supported in part by the National Natural Science Foundation of China under Grants 61635006, 11274224, and 61475098. The work of X. Zeng was supported by the Program for Professor of Special Appointment (Eastern Scholar) at Shanghai Institutions of Higher Learning and Science and Technology Commission of Shanghai Municipality (16520720900). The work of F. Pang was supported by "Shuguang Program" supported by Shanghai Education Development Foundation and Shanghai Municipal Education Commission (16SG35). *(Corresponding author: Xianglong Zeng.)*

The authors are with the Key Lab of Specialty Fiber Optics and Optical Access Network, Shanghai University, Shanghai 200072, China (e-mail: kingteng@shu.edu.cn; vangfeng@163.com; shifan_shu@163.com; ffpang@shu.edu.cn; sjhuang@shu.edu.cn; tywang@shu.edu.cn; zenglong@shu.edu.cn).

Color versions of one or more of the figures in this paper are available online at http://ieeexplore.ieee.org.

Digital Object Identifier 10.1109/JLT.2017.2676241

0733-8724 © 2017 IEEE. Personal use is permitted, but republication/redistribution requires IEEE permission.
See http://www.ieee.org/publications_standards/publications/rights/index.html for more information.

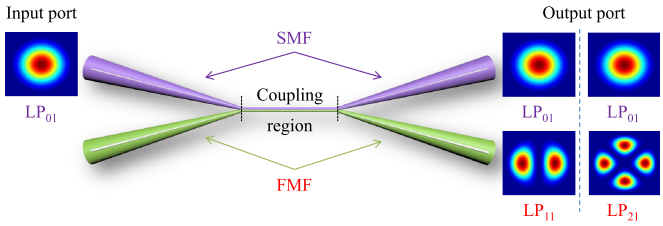

Fig. 1. Schematic of the MSCs, composed of a SMF and a FMF. Light is launched in the SMF input port; The LP_{11} (LP_{21}) mode is expected to be preferentially excited at the FMF output port, while the uncoupled fundamental LP_{01} mode will propagate along the SMF.

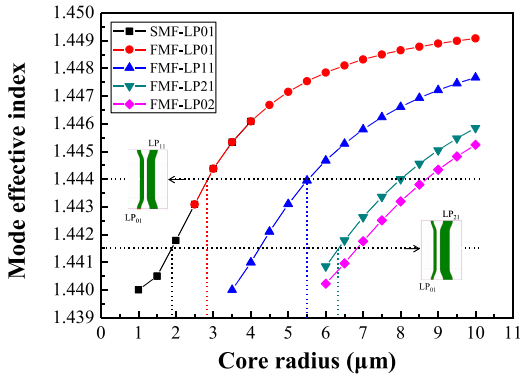

Fig. 2. The mode effective index curves for the LP_{01} in the SMF and the desired high-order modes in the FMF versus core radius at the wavelength of 1550 nm.

mode to LP_{11} (LP_{21}) mode within a wide bandwidth. The high-order optical vortex pulse can be obtained by using a polarization controller (PC) on the FMF output port [30].

II. Coupler Fabrication and Working Principle

Optical fiber couplers have a wide application in optical fiber communication systems. Both single-mode fiber (SMF) and few-mode fiber (FMF) couplers are commercially available to be used as optical splitters/combiners. The proposed SMF-FMF coupler can not only be used as a splitter, but also as a mode converter [31], [32].

A. SMF-FMF Coupler Simulation

Here, we present the schematic of SMF-FMF coupler which can excite high-order modes as shown in Fig. 1. The principle of the coupler is to phase match the fundamental mode in a single-mode fiber with a high-order mode in a few-mode fiber, and achieve mode conversion to high-order modes [31]. The larger the difference between these propagation constants, the lower the maximum power coupling efficiency. It is well known that the phase-matching condition can be achieved by satisfying the propagation constants of LP_{01} mode in the SMF with LP_{11} (LP_{21}) mode in the FMF according to the coupled-mode theory [33]. The propagating constants of different modes in SMF and FMF can be changed by pre-tapering the fiber diameters.

The phase-matching curves in Fig. 2 show the relationship between the mode effective indices and fiber diameters. The mode effective indices are calculated with the different fiber diameters for step-index fiber profiles. The thinner the core radius, the lower the mode effective index. Two phase-matching points are selected for the simulations, in which the SMF and FMF are both pre-tapered. The upper dotted line represents the fiber dimensions chosen for LP_{11} coupler, which indicates that the SMF should be set to a core/cladding diameter of 5.6/87.5 μm, and FMF should be set to a core/cladding diameter of 10.9/68.125 μm. The under dotted line represents the fiber dimensions chosen for LP_{21} coupler, which indicates that the SMF should be set to a core/cladding diameter of 3.85/60.156 μm, and FMF should be set to a core/cladding diameter of 12.8/80 μm. The optimum tapered diameters and the coupler length are obtained by optimizing the coupling efficiency in the experiment, until the desired mode and splitting ratio are achieved.

In order to determine the dependency of the coupling efficiency between the LP_{01} mode and high-order modes on the fiber tapering diameter, the following coupled equations are solved:

$$\frac{dA_1(z)}{dz} = i(\beta_1 + C_{11})A_1 + iC_{12}A_2 \tag{1}$$

$$\frac{dA_2(z)}{dz} = i(\beta_2 + C_{22})A_2 + iC_{21}A_1 \tag{2}$$

where z represents the distance along the coupling region of the coupler, A_1 and A_2 are the slowly-varying field amplitudes in the SMF and FMF of the fused coupler, β_1 and β_2 are the propagation constants of LP_{01} mode in the SMF and high-order mode in the FMF, respectively. To make LP_{01} mode in the SMF phase-matching with the desired high-order modes in the FMF, β_1 should be equal to β_2. C_{11} and C_{22}, C_{12} and C_{21} are the self-coupling and mutual coupling coefficients. Self-coupling coefficients are small relative to mutual coupling coefficients, and can be ignored, also $C_{12} \approx C_{21} \approx C$, where C depends on the width and length of coupling region. Thus, the power distributions in coupler are given by [34]:

$$P_1(z) = |A_1(z)|^2 = 1 - F^2 \sin^2\left(\frac{C}{F}z\right) \tag{3}$$

$$P_2(z) = F^2 \sin^2\left(\frac{C}{F}z\right) \tag{4}$$

where $F = [1 + \frac{\beta_1 - \beta_2}{4C^2}^2]^{-1/2}$, F^2 is the maximum coupling power between the two fiber. According to (3) and (4), it can find that power in coupling region exchanges periodically. This suggests that by choosing a suitable interaction length, any arbitrary power distribution between the two interacting waveguides can be achieved. When propagation distance equals to coupling length, the power of LP_{01} mode in SMF can be completely transferred to a certain higher-mode in FMF which meets the phase matching condition.

The commercial simulation software (Rsoft) is used to solve the modes propagating in the SMF-FMF couplers numerically and confirm the phase-matching condition as shown in Fig. 2. In our simulations, SMF core diameters are set to 5.60 μm, 3.85 μm for LP_{11}, LP_{21} couplers, FMF core diameters are set to 10.90 μm, 12.80 μm, respectively, the corresponding mode effective indices are 1.4440, 1.4415. And the coupling region

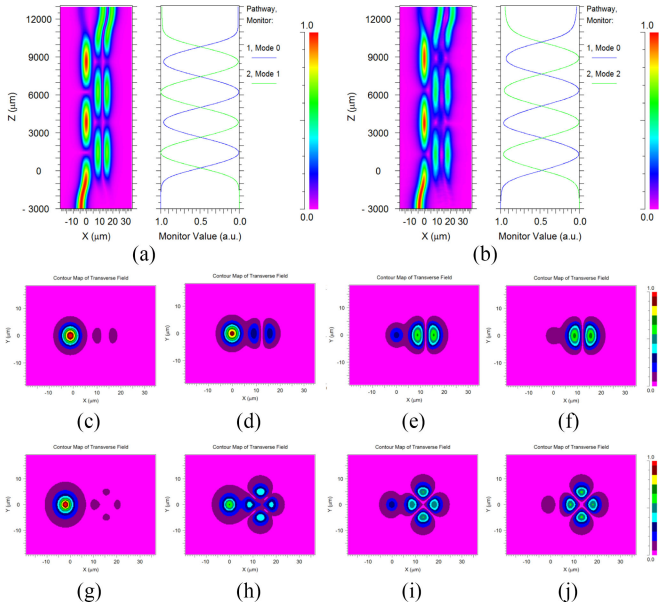

Fig. 3. Simulation results: (a) and (b): The power exchange in the coupling region when LP_{01} mode in SMF converts to LP_{11} (LP_{21}) mode in FMF; (c)–(f) and (g)–(j): The evolutions of mode field distribution in the coupling region when LP_{01} mode converts to LP_{11} (LP_{21}) mode in one period.

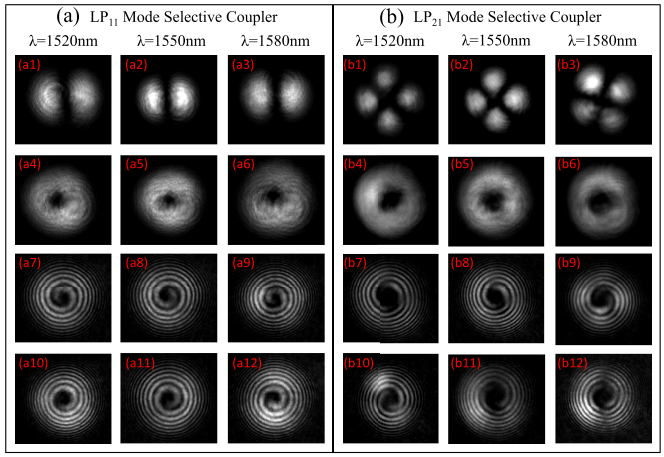

Fig. 4. CCD images of the output beam from mode selective couplers at wavelength of 1520 nm, 1550 nm and 1580 nm. (a1)–(a3) and (b1)–(b3): Intensity profiles of the LP_{11} and LP_{21} modes at the output FMF; (a4)–(a6) and (b4)–(b6): Donut-shaped mode patterns when pressing the output FMF; (a7)–(a12) and (b7)–(b12): Spiral interferograms of corresponding optical vortices.

length is set to 10 000 μm, the core distance between two fibers is set to 5 μm. From the simulation results, it is noticed that the power in coupling region exchanges periodically. Fig. 3(a) and (b) show the power exchange in the coupling region when LP_{01} mode in the SMF converts to LP_{11} (LP_{21}) mode in the FMF. Fig. 3(c)–(f) show the mode field distributions along the coupling region when LP_{01} mode converts to LP_{11} mode in one period. Fig. 3(g)–(j) show the mode field distributions when LP_{01} mode converts to LP_{21} mode in one period. The evolutions of mode field distribution in the coupling region clearly present efficient mode conversion from LP_{01} to desired high-order modes gradually.

B. Mode Conversion in SMF-FMF Coupler

A fused SMF-FMF fiber coupler basically consists of two parallel optical fibers that have been twisted, stretched and fused together by using oxyhydrogen flame so that their fiber cores are very close to each other. This forms a coupling region as shown in Fig. 1. The optical power couples from one fiber core to the other periodically in coupling region. The length of this coupling region determines the coupling ratio at given wavelength [34]. Optimum taper diameters are determined after experimental fine tuning of pre-tapered SMF diameters. According to our experimental results, SMF (core/cladding diameter = 8/125 μm) is pre-tapered to diameters of 85 μm, 50 μm, respectively. The insertion loss of the pre-tapered fiber is measured to be smaller than 0.1 dB. The pre-tapered SMF fiber is then fused to the FMF (core/cladding diameter = 20/125 μm) until the power transfer between two output ports is maximized.

During the fusing process, light is launched into the input port, and the output powers from the output ports are carefully monitored. When the desired coupling ratio (90:10, FMF port is 10) is achieved, the fully automated fusing process is stopped. The power is redistributed in the coupler region, and LP_{11} (LP_{21}) mode is able to dominate in the output of FMF due to the phase-matching condition. Lastly, the fused SMF-FMF coupler is encapsulated by using epoxy resin adhesive and heat shrink tubing. The excess loss of LP_{11} and LP_{21} SMF-FMF couplers are measured to be 0.4 dB, 2.5 dB, respectively.

When the FMF is not deformed, the output beam is a high-order (LP_{11} or LP_{21}) mode beam. Linearly polarized (LP) modes can be regarded as the superposition of vector modes. Fiber OAM modes can be obtained by combining different vector modes $HE_{2,m}^{even}$ ($HE_{2,m}^{odd}$) and $TE_{0,m}$ ($TM_{0,m}$) when $l = 1$ or combining $HE_{l+1,m}^{even}$ ($HE_{l+1,m}^{odd}$) and $EH_{l-1,m}^{odd}$ ($EH_{l-1,m}^{even}$) when $l > 1$ with a $\pi/2$ phase shift, where l refers to the azimuthal index and m refers to the radial index [35]. In order to generate OAM modes in weakly guiding fibers, production of a $\pi/2$ phase shift between the two vector modes becomes a key issue. Shuhui Li *et al.* proposed a simple method to generate the phase shift by using a rotator and a flat slab [30]. This is because the stress changes the effective dimensions of the FMF, leading to different phase velocities of the two modes. A polarization controller (PC) is used to replace the rotator and flat slab. By rotating the PC3 and adjusting the pressure appropriately, the two vector modes can achieve a $\pi/2$ phase shift, and the output is an OAM beam with a circularly symmetric annular intensity profile and a helical phase front.

In order to verify the mode selective coupler with a broad bandwidth, the output LP_{11} and LP_{21} mode patterns and corresponding interference patterns of OAM modes are observed from 1520 nm to 1580 nm. The mode selections have a better performance at the communication wavelength of 1550 nm. Some experimental results of LP_{11} and LP_{21} mode selective coupler are shown in Fig. 4(a) and (b), respectively. The output beam profiles are recorded by using a CCD camera (InGaAs camera, Model C10633-23 from Hamamtsu Photonics).

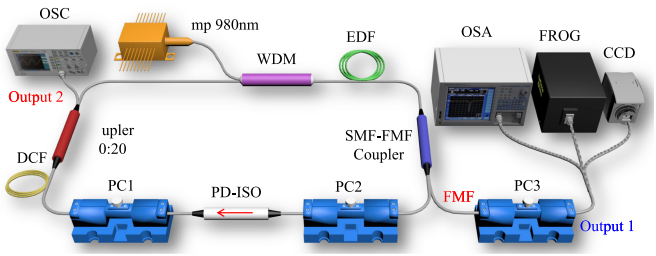

Fig. 5. Experimental setup used to excite OVB pulse. WDM: Wavelength Division Multiplexing coupler; EDF: Erbium-doped Fiber; DCF: Dispersion Compensating Fiber; PC: Polarization Controller; PD-ISO: Polarization-dependent Isolator; FROG: Frequency-resolved Optical Gating; OSC: Oscilloscope; OSA: Optical Spectrum Analyzer; CCD: Charge Coupled Device, Infrared camera.

As shown in the first row, the experimental near-field patterns of LP_{11} mode and LP_{21} mode are successfully excited. The near-filed beam profiles show that the fused SMF-FMF coupler can work as a all-fiber mode-converter from LP_{01} mode to LP_{11} (LP_{21}) mode with a broadband width, i.e., mode selective couplers can support spectral widths of femtosecond pulse. The second row shows the corresponding donut-shaped patterns when pressing the output FMF port. The last two rows show the interference patterns of the donut-shaped beams with a reference Gaussian beam, which indicates that the donut-shaped beams are vortex beams and the topological charge of vortices to be 1, 2, respectively. The clockwise spiral interference patterns for OAM_{-1}, OAM_{-2} and the counterclockwise spiral interference patterns for OAM_{+1}, OAM_{+2} clearly indicate that $OAM_{\pm 1}$ and $OAM_{\pm 2}$ are successfully achieved at the output FMF port.

III. Experiments and Discussion

Passively mode-locked fiber laser is to generate ultra-short optical pulses with femtosecond pulse duration. Mode-locking in a fiber cavity is typically based on saturable absorption (SA) [36], [37] and NPR [38], in which a model including the nonlinear Schrödinger equation is useful to understand the pulse propagating in the cavity. To gain shorter pulse, our experimental setup is based on NPR. The schematic setup of a MLFL with ultrafast OVBs is shown in Fig. 5. The fused SMF-FMF fiber couplers are inserted in the mode-locked cavity of fiber laser to generate femtosecond pulses. The NPR mode-locking can be easily initialized by adjusting the PCs in the cavity. The mode selective couplers are inserted into the fiber laser to excite LP_{11} (LP_{21}) mode into FMF and femtosecond OVBs with $l = \pm 1$ or 2 are successfully excited in Output 1.

A length of 0.4 m heavily doped erbium-doped fiber (EDF) (LIEKKI, ER80-8/125) with group velocity dispersion of -20 ps^2/km is used in the experiment. The EDF with peak absorption of 80 dB/m at 1530 nm is acted as a gain medium. And it is pumped by a 980 nm laser diode with a maximum pump power of 620 mW through 980/1550 nm wavelength division multiplexing coupler (WDM). A length of 1.5 m dispersion compensating fiber (DCF) (THORLABS, DCF38) with group velocity dispersion of 50.35 ps^2/km is used to compensate negative dispersion fiber. A polarization-dependent isolator (PD-ISO) is

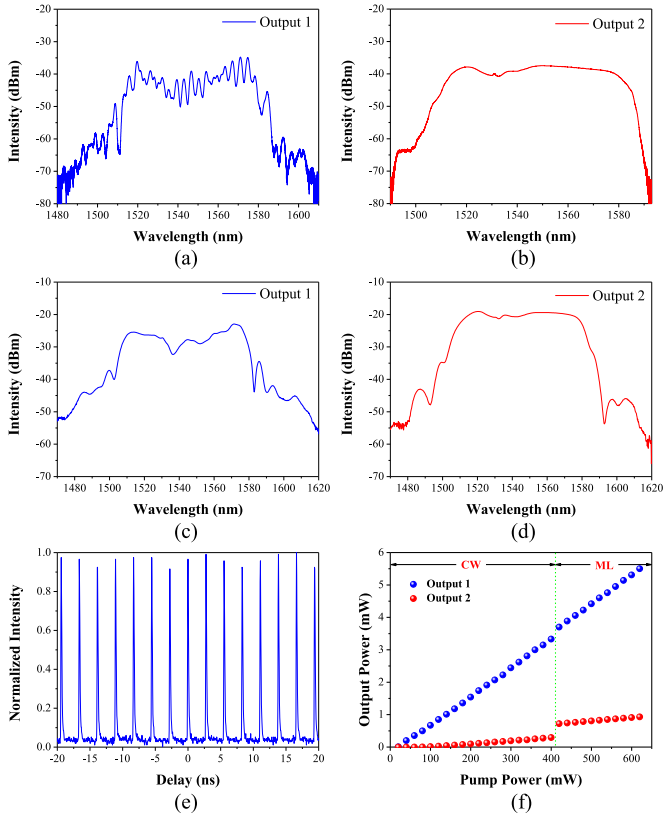

Fig. 6. (a) and (b): Spectra of LP_{11} mode in Output 1 at pump power of 620 mW and the corresponding spectrum at Output 2. (c) and (d): Spectra of LP_{21} mode in Output 1 at pump power of 620 mW and the corresponding spectrum at Output 2. (e): Mode-locked pulse trains of femtosecond $OAM_{\pm 2}$ mode. (f): The output powers from Output 1 and Output 2 as the function of pump power when mode selective coupler excited $OAM_{\pm 2}$ mode.

inserted in the laser cavity to force the unidirectional laser operation and acts as the polarizer for the NPR mode-locking. The 80:20 optical coupler (OC) is used to extract the energy in the cavity for monitoring. The fused SMF-FMF coupler (90:10) acts as power splitter and mode converter. Two polarization controllers (PCs) in the cavity are used to optimize the NPR. All the devices in the cavity are connected by standard SMF with GVD of -23 ps^2/km at 1550 nm. The total cavity length is 5.9 m, and the net cavity dispersion is 0.015 ps^2. The output spectrum is analyzed by an optical spectrum analyzer (YOKOGAWA, AQ6370C), and the time domain waveform is recorded by a 10 GHz electro-photonic detector (CONQUER, KG-PD-10G-FP) followed with a 1 GHz oscilloscope (Tektronix, MSO 4104). The signal is also sent to a commercial frequency-resolved optical gating (FROG, Mesa Photonics) for characterizing the pulse duration and the spectrum.

Firstly, an oscilloscope and optical spectrum analyzer (OSA) are used to observe the pulse trains and analyze the output spectrum, as shown in Fig. 6. The working state of fiber laser is monitored by using the signal of Output 2. Output 1 is analyzed under a pump power of 620 mW. Fig. 6(a) and (b) show the output spectra when using LP_{11} coupler. A typical broad bandwidth spectrum is observed in Fig. 6(a) due to the

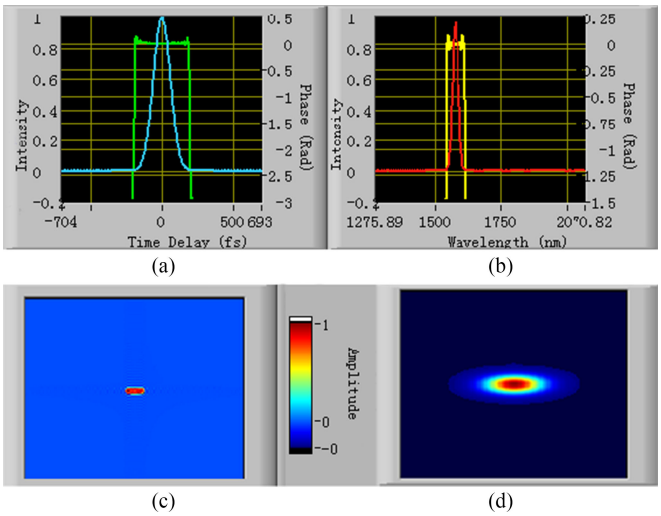

Fig. 7. FORG results of vortex pulses with $OAM_{\pm 2}$: (a) Temporal intensity and phase profile, (b) spectral intensity and phase profile, (c) Measured FROG traces, (d) Retrieved FROG traces.

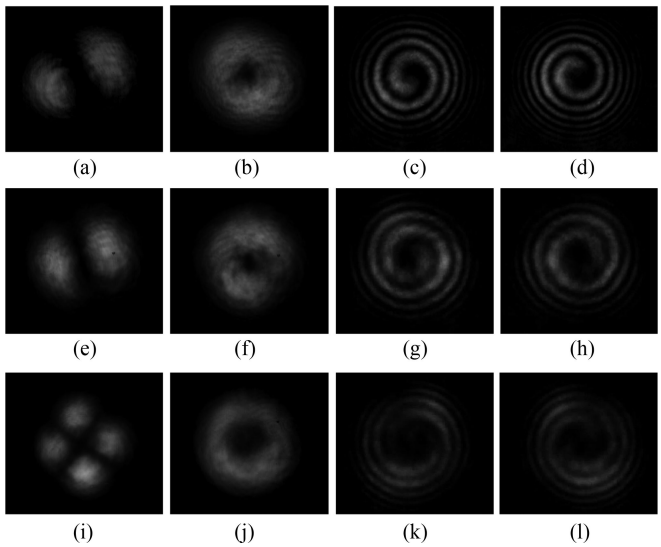

Fig. 8. CCD images of near-field intensity distribution of Output 1. (a), (e), and (i): Intensity profiles of the LP_{11} and LP_{21} modes at the output FMF; (b), (f), and (j): Donut-shaped mode patterns when pressing the output FMF; (c), (d), (g), (h), (k), and (l): Corresponding spiral interferograms. The first row shows the near-field intensity distributions when the fiber laser is running at the state of CW. Both second and third rows show the near-field intensity distributions when the fiber laser is running at the state of ML.

positive net dispersion in the cavity [29]. The central wavelength locates at 1547.4 nm, and the 3-dB bandwidth is measured to be 56.5 nm. The interference fringes in the FMF port are caused by the interference between the degenerated vector modes of LP_{11} mode. LP_{11} mode is degenerated by four vector modes possessing similar propagation constants, including TE_{01}, TM_{01}, HE_{21}^{odd} and HE_{21}^{even}. Fig. 6(c) and (d) show the spectra of Output 1 and 2 when using LP_{21} coupler. The central wavelength locates at 1545 nm, and the 3-dB bandwidth is measured to be 67.6 nm at Output 1. When LP_{11} coupler (LP_{21} coupler) is inserted into the cavity, the total insert loss of the fiber laser cavity is 1.1 dB (3.2 dB). Fig. 6(e) presents the pulse trains of Output 1 with repetition rate of 36.10 MHz when using LP_{21} coupler. Fig. 6(f) shows the evolution of the output power versus the pump power for $OAM_{\pm 2}$ mode. It is noticed that fiber laser is working at the CW state when the pump power is below 420 mW. Increasing the pump power continuously, self-starting and stable mode-locking is able to operate.

Secondly, a FROG is used to measure the pulse duration of OVBs with $OAM_{\pm 1}$ and $OAM_{\pm 2}$. The temporal and spectral intensities, phase profiles, frequency-doubled second harmonic generation (SHG) signal, the measured and retrieved FROG traces of the pulse from Output 1 are illustrated in Fig. 7. The pulse durations of $OAM_{\pm 1}$ and $OAM_{\pm 2}$ beams are measured to be 273 fs, 140 fs, respectively. And the time bandwidth product both are 0.45 from the retrieved signal.

The fused SMF-FMF coupler is verified effectively when acting as a mode converter. The mode patterns from Output 1 are observed when the fiber laser is running at the state of CW and ML. A polarizer is added before CCD camera, by rotating the polarization direction, linearly polarized vortex beams are realized. As shown in Fig. 8, the experimental near-field patterns of LP_{11} and LP_{21} modes and the corresponding $OAM_{\pm 1}$ and $OAM_{\pm 2}$ modes are successfully obtained. Fig. 8(a)–(d) show the near-field intensity distributions when the fiber laser is running at the state of CW. Fig. 8(a) and (b) are the experimental near-field patterns of LP_{11} mode and donut-shaped mode pattern when adjusting the PC3 on the FMF. Fig. 8(c) and (d) are the corresponding spiral interferogram. Fig. 8(e)–(l) show the near-field intensity distributions when the fiber laser is running at the state of ML. Fig. 8(e) and (i) show the experimental near-field patterns of LP_{11} and LP_{21} modes are successfully excited. Donut-shaped mode patterns of LP_{11} and LP_{21} modes are shown in Fig. 8(f) and (j). Efficient mode coupling occurs and different vector modes with polarization state are easily excited by adjusting the PC3 based on the principle of extrusion and torsion [30]. The intra-cavity PCs are carefully adjusted to obtain ideal OVBs for ensuring the mode-locking operation. Fig. 8(g), (h), (k), and (l) show the interference patterns of the donut-shaped beams with Output 2 (as a reference Gaussian beam), which indicates that femtosecond donut-shaped beams are vortex beams and the topological charge of vortices to be 1, 2, respectively. The clockwise spiral interference patterns for OAM_{-1}, OAM_{-2} and the counter-clockwise spiral interference patterns for OAM_{+1}, OAM_{+2} can be clearly seen, which shows that femtosecond $OAM_{\pm 1}$ and $OAM_{\pm 2}$ are successfully achieved at the output FMF port.

IV. Conclusion

In conclusion, we show that mode selective couplers can be used to generate high-order OVBs and mode couplings is analyzed in the coupling region between the fundamental mode in SMF and a high-order mode in FMF. We experimentally demonstrate an all-fiber optical vortex MLFL based on the mode selective coupler, and femtosecond optical vortex beams with topological charge of 1 and 2 are obtained from FMF output

port of mode selective couplers, respectively. To the best of our knowledge, this is the first time to demonstrate such ultrafast MLFL supporting the generation of OVBs pulse by using the mode selective coupler. The measured time duration of OVB pulses are 273 fs, 140 fs of $OAM_{\pm 1}$ and $OAM_{\pm 2}$. The maximum single pulse energy we obtain is 0.36 nJ and can be improved by increasing the pump power or reducing the excess loss of SMF-FMF coupler. Such ultrafast vortex beams can be used to fabricate a chiral nano-structure originated by angular momentum transfer of the optical vortex to a material. A shorter pulse of the MLFL is supposed to be implemented by optimizing the dispersion of the laser cavity.

REFERENCES

[1] L. Allen, M. W. Beijersbergen, R. Spreeuw, and J. Woerdman, "Orbital angular momentum of light and the transformation of Laguerre-Gaussian laser modes," *Physical Rev. A*, vol. 45, no. 11, pp. 8185–8189, 1992.

[2] L. Allen, M. Padgett, and M. Babiker, "IV the orbital angular momentum of light," *Progress Opt.*, vol. 39, pp. 291–372, 1999.

[3] M. Padgett and R. Bowman, "Tweezers with a twist," *Nature Photon.*, vol. 5, no. 6, pp. 343–348, 2011.

[4] H. Kawauchi, K. Yonezawa, Y. Kozawa, and S. Sato, "Calculation of optical trapping forces on a dielectric sphere in the ray optics regime produced by a radially polarized laser beam," *Opt. Lett.*, vol. 32, no. 13, pp. 1839–1841, 2007.

[5] H. Arnaut and G. Barbosa, "Orbital and intrinsic angular momentum of single photons and entangled pairs of photons generated by parametric down-conversion," *Physical Rev. Lett.*, vol. 85, no. 2, pp. 286–289, 2000.

[6] J. Wang *et al.*, "Terabit free-space data transmission employing orbital angular momentum multiplexing," *Nature Photon.*, vol. 6, no. 7, pp. 488–496, 2012.

[7] N. Bozinovic *et al.*, "Terabit-scale orbital angular momentum mode division multiplexing in fibers," *Science*, vol. 340, no. 6140, pp. 1545–1548, 2013.

[8] A. E. Willner *et al.*, "Optical communications using orbital angular momentum beams," *Adv. Opt. Photon.*, vol. 7, no. 1, pp. 66–106, 2015.

[9] C. Hnatovsky, V. G. Shvedov, W. Krolikowski, and A. V. Rode, "Materials processing with a tightly focused femtosecond laser vortex pulse," *Opt. Lett.*, vol. 35, no. 20, pp. 3417–3419, 2010.

[10] M. Koyama, T. Hirose, M. Okida, K. Miyamoto, and T. Omatsu, "Power scaling of a picosecond vortex laser based on a stressed Yb-doped fiber amplifier," *Opt. Express*, vol. 19, no. 2, pp. 994–999, 2011.

[11] K. Toyoda, K. Miyamoto, N. Aoki, R. Morita, and T. Omatsu, "Using optical vortex to control the chirality of twisted metal nanostructures," *Nano Lett.*, vol. 12, no. 7, pp. 3645–3649, 2012.

[12] K. Toyoda *et al.*, "Transfer of light helicity to nanostructures," *Physical Rev. Lett.*, vol. 110, no. 14, 2013, Art. no. 143603.

[13] F. Takahashi, K. Miyamoto, H. Hidai, K. Yamane, R. Morita, and T. Omatsu, "Picosecond optical vortex pulse illumination forms a monocrystalline silicon needle," *Sci. Rep.*, vol. 6, 2016, Art. no. 21738.

[14] M. Beijersbergen, R. Coerwinkel, M. Kristensen, and J. Woerdman, "Helical-wavefront laser beams produced with a spiral phase plate," *Opt. Commun.*, vol. 112, no. 5, pp. 321–327, 1994.

[15] A. S. Ostrovsky, C. Rickenstorff-Parrao, and V. Arrizón, "Generation of the 'perfect' optical vortex using a liquid-crystal spatial light modulator," *Opt. Lett.*, vol. 38, no. 4, pp. 534–536, 2013.

[16] N. Heckenberg, R. McDuff, C. Smith, and A. White, "Generation of optical phase singularities by computer-generated holograms," *Opt. Lett.*, vol. 17, no. 3, pp. 221–223, 1992.

[17] M. Beijersbergen, L. Allen, H. Van der Veen, and J. Woerdman, "Astigmatic laser mode converters and transfer of orbital angular momentum," *Opt. Commun.*, vol. 96, no. 1–3, pp. 123–132, 1993.

[18] P. Gregg *et al.*, "Q-plates as higher order polarization controllers for orbital angular momentum modes of fiber," *Opt. Lett.*, vol. 40, no. 8, pp. 1729–1732, Apr. 2015.

[19] Z. Lin *et al.*, "Generation of optical vortices using a helical fiber Bragg grating," *J. Lightw. Technol.*, vol. 32, no. 11, pp. 2152–2156, Jun. 2014.

[20] X. Zhang, A. Wang, R. Chen, Y. Zhou, H. Ming, and Q. Zhan, "Generation and conversion of higher order optical vortices in optical fiber with helical fiber Bragg gratings," *J. Lightw. Technol.*, vol. 34, no. 10, pp. 2413–2418, May 2016.

[21] Y. Zhao, Y. Liu, L. Zhang, C. Zhang, J. Wen, and T. Wang, "Mode converter based on the long-period fiber gratings written in the two-mode fiber," *Opt. Express*, vol. 24, no. 6, pp. 6186–6195, 2016.

[22] N. Bozinovic, S. Golowich, P. Kristensen, and S. Ramachandran, "Control of orbital angular momentum of light with optical fibers," *Opt. Lett.*, vol. 37, no. 13, pp. 2451–2453, 2012.

[23] Y. Yan *et al.*, "Fiber coupler for generating orbital angular momentum modes," *Opt. Lett.*, vol. 36, no. 21, pp. 4269–4271, 2011.

[24] S. Pidishety, M. A. Khudus, P. Gregg, S. Ramachandran, B. Srinivasan, and G. Brambilla, "OAM beam generation using all-fiber fused couplers," in *Proc. CLEO, Sci. Innovations*, 2016, Paper STu1F–2.

[25] J. Li, K.-i. Ueda, M. Musha, L. Zhong, and A. Shirakawa, "Radially polarized and pulsed output from passively q-switched nd: Yag ceramic microchip laser," *Opt. Lett.*, vol. 33, no. 22, pp. 2686–2688, 2008.

[26] D. Lin *et al.*, "Efficient, high-power, and radially polarized fiber laser," *Opt. Lett.*, vol. 35, no. 13, pp. 2290–2292, 2010.

[27] D. Lin *et al.*, "Radially polarized and passively q-switched fiber laser," *Opt. Lett.*, vol. 35, no. 21, pp. 3574–3576, 2010.

[28] J. Dong and K. S. Chiang, "Mode-locked fiber laser with transverse-mode selection based on a two-mode FBG," *IEEE Photon. Technol. Lett.*, vol. 26, no. 17, pp. 1766–1769, 2014.

[29] D. Deng, L. Zhan, Z. Gu, Y. Gu, and Y. Xia, "55-fs pulse generation without wave-breaking from an all-fiber erbium-doped ring laser," *Opt. Express*, vol. 17, no. 6, pp. 4284–4288, 2009.

[30] S. Li, Q. Mo, X. Hu, C. Du, and J. Wang, "Controllable all-fiber orbital angular momentum mode converter," *Opt. Lett.*, vol. 40, no. 18, pp. 4376–4379, 2015.

[31] R. Ismaeel, T. Lee, B. Oduro, Y. Jung, and G. Brambilla, "All-fiber fused directional coupler for highly efficient spatial mode conversion," *Opt. Express*, vol. 22, no. 10, pp. 11 610–11 619, 2014.

[32] S. Pidishety, B. Srinivasan, and G. Brambilla, "All-fiber fused coupler for stable generation of radially and azimuthally polarized beams," *IEEE Photon. Technol. Lett.*, vol. 29, no. 1, pp. 31–34, Jan. 2016.

[33] K. J. Park, K. Y. Song, Y. K. Kim, J. H. Lee, and B. Y. Kim, "Broadband mode division multiplexer using all-fiber mode selective couplers," *Opt. Express*, vol. 24, no. 4, pp. 3543–3549, 2016.

[34] X. Ya-Ling, L. Yan-Ge, W. Zhi, L. Xiao-Qi, and L. Ming-Ming, "Design and experimental study of mode selective all-fiber fused mode coupler based on few mode fiber," *Acta Physica Sinica*, vol. 64, no. 20, 2015, Art. no. 204207.

[35] Y. Jiang, G. Ren, Y. Lian, B. Zhu, W. Jin, and S. Jian, "Tunable orbital angular momentum generation in optical fibers," *Opt. Lett.*, vol. 41, no. 15, pp. 3535–3538, 2016.

[36] D. Tang, H. Zhang, L. Zhao, and X. Wu, "Observation of high-order polarization-locked vector solitons in a fiber laser," *Physical Rev. Lett.*, vol. 101, no. 15, 2008, Art. no. 153904.

[37] H. Zhang, D. Tang, L. Zhao, X. Wu, and H. Tam, "Dissipative vector solitons in a dispersion managed cavity fiber laser with net positive cavity dispersion," *Opt. Express*, vol. 17, no. 2, pp. 455–460, 2009.

[38] B. Oktem, C. Ülgüdür, and F. O. Ilday, "Soliton similariton fibre laser," *Nature Photon.*, vol. 4, no. 5, pp. 307–311, 2010.

Authors' biographies not available at the time of publication.

152.78.74.132 [ts 2018-05-15 12:36:48]